Towards Ultrasound-Assisted Dosimetry using Photon/Proton Activable Poly(vinylalcohol) Phase Change Nanodroplets: A Concept Study

YosraToumia[1], Roberto Miceli[2], Fabio Domenici[1], MadalinaCociorb[1,3], Letizia Oddo[1], Piero Rossi[4], Sophie V. Heymans[5,6], BramCarlier[7], Rolando Maria D'Angellilo[2], Edmond Sterpin[7], Emiliano D'Agostino[3], Koen Van Den Abeele[5], Jan D'Hooge[6], Gaio Paradossi[1]

[1] *Department of Chemical Science and Technology, University of Rome Tor Vergata, Itaky*
[2]*UOC Radiotherapy, Department of Oncology, Policlinico Tor Vergata (PTV), University of Rome Tor Vergata, Italy*
[3]*DoseVue, Hasselt, Belgium*
[4]*Department of Experimental Medicine and Surgery, PTV, University of Rome Tor Vergata, Italy*
[5]*Department of Physics, KU Leuven Campus Kulak, Kortrijk, Belgium*
[6]*Department of Cardiovascular Sciences, KU Leuven, Leuven, Belgium*
[7]*Department of Oncology, KU Leuven, Leuven, Belgium*

ABSTRACT

Phase-change nanodroplets (NDs) consist of injectable contrast agents for ultrasound imaging, able to vaporize to echogenic microbubbles upon an acoustic or optical activation. Herein, we investigate nanodroplets vaporization in a particular process using ionizing radiations for dosimetry in radiotherapy applications. We investigated novel low boiling point (b.p.) NDs stabilized with a poly(vinylalcohol) (PVA) shell. A physico-chemical characterization of NDs, as well as their acoustic transition into MBs have been first assessed. Then, we addressed the effect of several parameters influencing nanodroplets radiation sensitivity such as beam type, energy, delivered dose and the core. The NDs, being dispersed in a hydrogel tissue-mimicking phantoms, are exposed either to X-ray photons at different medical doses and energies or to a proton beam for comparison. The ultrasound imaging of the phantoms pre- and post-radiation reveal a clear radiation-induced droplet vaporization at clinically relevant doses. More efficiently, vaporization events occur with protons than with photons due to high linear energy transfer (LET) recoils produced by nuclear reaction with incoming protons.

1. INTRODUCTION

Conventional radiotherapy applies ionizing radiation high doses to kill or slow the growth of malignant tumor cells and is considered as one of the major therapeutic approaches among cancer treatments. This approach is referring to an external beam exposure and often uses X-ray beams to locally treat the cancerous tissues. Linear accelerators, known as 'linac', are employed to produce X-ray photons at various energies, which define the dose penetration depth into the target tissue (Mohan et al., 2019; Baskar et al., 2012). Typically, modern beams operate in the energy range of 4-20 MV and generate MeV photons. During a radiation treatment, the X-ray photons first deposit

a certain dose on the patient skin. Subsequently, as they penetrate the body, the delivered dose rise rapidly to reach its maximum at a certain depth, then declines exponentially (Roser et al., 2019). Recently, charged particle beams such as protons and carbon ions became clinically accessible (i.e. hadron therapy) in a continuous efforts aiming to increase the number of therapeutic options (Amaldi, 1999). The hadron therapy is considered more beneficial in treating cancers which are nearby critical organs (e.g. breast cancer), as unlikely to x-ray photons, the charged particles diffuse less when penetrating the tissues and deposit a maximum energy just before extinguishing known as the "Bragg peak" (Mohan et al., 2013; Opalka et al., 2012). However, the main challenges for a correct radiotherapy plan remain patient *in-situ* dosimetry and radiation delivery verification, which can be achieved with the control of the absorbed energy and its spatial distribution. These considerations potentially allow for better tumor control and lower the damages on the surrounding healthy tissues, while a poorly estimated delivery plan might lead to an opposite outcome with undesired biological effects (Bloemen-van Gurp et al., 2007; Mohan et al., 2019). Numerous dosimetry technologies are used in the clinical field, ranging from gafchromic films to scintillation detectors (Archambault et al., 2006; Beaulieu et al., 2013; Butson et al., 2003; Casolaro et al., 2019; Parwaie et al., 2018; Piermattei et al., 2007). However, all these current dose assessment methods remain rudimentary and generally consist of offline measurements or point verifications limited to the patient's skin. Bubble chambers are common detectors for ionizing radiation used in different fields, e.g. neutron science and medical physics (Roy, 2001); the first was achieved several decades ago by Glaser for the detection of charged particles (Glaser, 1952). These latter consist of emulsions of superheated droplets, i.e. in a metastable state above their boiling point. External stimuli, such as physical stresses (i.e. shear), temperature increasing or radiation exposure, rise the probability of nucleation within a superheated liquid, inducing its vaporization. However, the nucleation strongly depends on the reduced superheat degree, s, defined as its 'driving force' (d'Errico et al., 2000; d'Errico (INVITED), 1999) in eq. 1:

$$s = \frac{T - T_b}{T_c - T_b} \quad (1)$$

where T_b is the boiling point of the liquid, T_c is the critical temperature and T is the experimental temperature.

Therefore, the higher is the degree of reduced superheat the more the droplets are susceptible to vaporize. The limit temperature of superheat degree (sl) upon which droplets can no longer exist at the metastable liquid state can be derived from empirical model equation (2) and equation (1) (Reid, 1983; Salla et al., 2006).

$$T_{sl}=T_c[0.11(P/Pc) + 0.89] \quad (2)$$

where T_{sl} is the superheat limit temperature, P is the pressure, P_c and T_c are critical pressure and temperature, respectively.

The majority of these detectors reported in the literature are uncoated microdroplets entrapped in polymeric or aqueous matrixes, and whose sizes range from tens to few thousands of micron (D'Enrico, 2001; Mondal et al., 2014). Depending on their superheat degree, the metastable droplets require a sufficient linear energy transfer (LET) to vaporize into bubbles when exposed to radiation. For example, Zacek et.al demonstrated that α radiation triggered complete phase transition of uncoated feron-12 droplets (b.p. -30°C) at a temperature above 35°C (Zacek, 1994). Such process can be typically detected visually, by a volumetric measurement or an acoustic readout. Two decades ago, Apfel envisioned the use of injectable superheated emulsions as *in vivo* dosimeter (Apfel, 1998), but to our knowledge, the idea has never been developed. Similar to the superheated emulsions, injectable sub-micrometer sized phase change contrast agents provide a novel means that deploy ultrasound imaging (US), and consist of a liquid perfluorocarbon core (PFC) stabilized by a lipid or polymer shell. Most commonly, echogenicity of PFC nanodroplets (NDs) is triggered by an acoustic or optical droplet vaporization processes, i.e. ADV or ODV, respectively (Sheeran et al., 2013b; Wilson et al., 2012) . Various PFCs have boiling points (b.p.) close to physiological temperatures, which allows for the design of droplets in or near a superheated state. However, in order to gain sensitivity of phase change NDs to clinical ionizing radiation, very low b.p. PFCs are required. In two recent studies, we have reported the first proof of concept on radiation-induced nanodroplets vaporization for proton range verification, by using perfluorobutane nanodroplets (PFB: b.p = -2°C) with i) crosslinked thin lipid shell, i.e. 10,12-pentacosadiynoic acid (PCDA) (Carlier et al., 2020), and ii) crosslinked poly(vinyl-alcohol) (PVA) (Heymans et al., 2020). The feasibility of the concept was demonstrated for both formulations, with a reproducible range shift <1mm, and the importance of superheat degree in affecting NDs response to radiation was elucidated by increasing the temperature. Herein we extend the previous work to address the physico-chemical properties of PVA shelled nanodroplets (PVA/PFB) and we correlate them with the transition ability of NDs, and to further evaluate their interaction with X-ray photon by ultrasound imaging. Moreover, we attempted to increase the superheat degree of NDs by changing the core to a lower boiling point PFC (b.p=-15°C). The advantage of monitoring radiation response with standard US imaging systems is, in perspective, an easy and non-invasive real-time dosimetry during an irradiation treatment.

The PVA shell has been suggested to provide an enhanced stability to the encapsulated droplets, in order to increase their life-time at physiological conditions. Besides, PVA-based polymer systems have been considered in the development of smart devices with multifunctional/tunable properties. In this respect, long established fields of application are the pharmaceutical and biomedical industries, where PVA has been extensively used as a privileged polymer for different kinds of encapsulation/loading due to its biocompatibility and good chemical versatility.(Gaaz et al., 2015; Jiang et al., 2011; Paradossi et al., 2003) This allows to consider shell functionalization in future with ligands for in *vivo* targeting by tethering tumor specific antibodies or peptides (Brooks et al., 2010; Oddo et al., 2017; Sánchez-Martín et al., 2013).

2. EXPERIMENTAL SECTION

2.1.Materials:

The following materials were purchased from Sigma-Aldrich (Milan, Italy) and used without further purification: poly(vinyl alcohol), PVA, (M_n = 30 ± 5 and M_w = 70 ± 10 kg/mol), sodium metaperiodate ($NaIO_4$), Dulbecco's modified Eagle's medium (DMEM), N,N'-methylenebisacrylamide (BIS) and ammonium persulfate (APS). Acrylamide (AM) and tetramethylethylenediamine (TEMED) were purchased from Bio-rad (Milan, Italy). Perfluorobutane (PFB) and 2-H heptafluoropropane (HFP) were purchased from Apollo Scientific (UK). Milli-Q, mQ, quality water (18.2 MΩ·cm) was produced using a deionization apparatus Pure Lab from USF (Rome, Italy). Customized rectangular phantom cans (inner dimensions: length = 54 mm, width = 26 mm, depth = 31 mm) were provided by KU Leuven (Belgium).

2.2.Methods

2.2.1. PVA/PFB nanodroplets preparation

Nandroplets are prepared by crosslinking telechelic PVA chains at the PFB/water interface: in brief, PVA powder is dissolved at 80°C in mQ water at a concentration of 2%(w/v). Then, $NaIO_4$, is added at 2% (mol:mol) with respect to a PVA repeating unit. The solution is kept under stirring for 1h to oxidize the head-to-head sequences present as structural defects in the PVA chain (Barretta et al., 2000), leading to the polymer splitting into shorter chains with aldehyde groups as terminals. Perfluorobutane (b.p. -2°C) is liquefied by fluxing it for few seconds in an empty glass vial sealed with a rubber septum, immersed in liquid nitrogen. Quickly, 5 ml of PVA solution are injected into the vial through the rubber using a syringe and the mixture is immediately sonicated for 15 min at 100 % power using an ice-cold ultrasonic bath cleaner (200W, 40 kHz, Ceia CP104, Florence, Italy). Sonication induces encapsulation of the liquid PFB during the crosslinking acetalization to form the PVA shell between aldehyde and hydroxyl groups. The nanodroplets are

left at 4°C for 1 hour prior to their washing to continue statically the crosslinking process .Finally, the PVA/PFB nanodroplets can be sorted by size and washed with mQ water by centrifugation (2500 rpm /1020 g; 5000 rpm/4080 g rcf, 5min) and stored at 4°C.

2.2.2. PVA/HFP nanodroplets preparation

Preparation of PVA/HFP nandroplets occurs via the same chemical process described in section 2.2.1, i.e. by crosslinking telechelic PVA chains at the HFP/water interface. Due to the lower boiling point (b.p =-15°C) of HFP than PFB, an *ad hoc* customized setup was built up in our laboratory allowing for pressure holding (see Scheme 1). A stainless steel reactor (volume 300 ml) with a cover head bearing two opening tube connections (i.e. for each HFP gas and PVA solution), and assembled to a dispersing tool T65 (IKA, Italy), is sealed via a stainless steel threaded ring and immersed in liquid nitrogen. The valves connecting the gas tube are opened and HFP is fluxed for 1 min. The reactor is kept immersed in the liquid nitrogen for another 2 min after fluxing to ensure complete liquefaction of HFP. After that, the reactor is left to thermally equilibrate at RT for 15 minutes before introducing the PVA solution in order to avoid its freezing. Once PVA is injected through a connected syringe into the reactor (V=70 ml), the latter is assembled to an Ultra-Turrax homogenizer motor (IKA, Germany) and the mixture is vigorously stirred at 9000 rpm for 15 min. Finally, the nanodroplets are collected in vials and stored at 4°C.

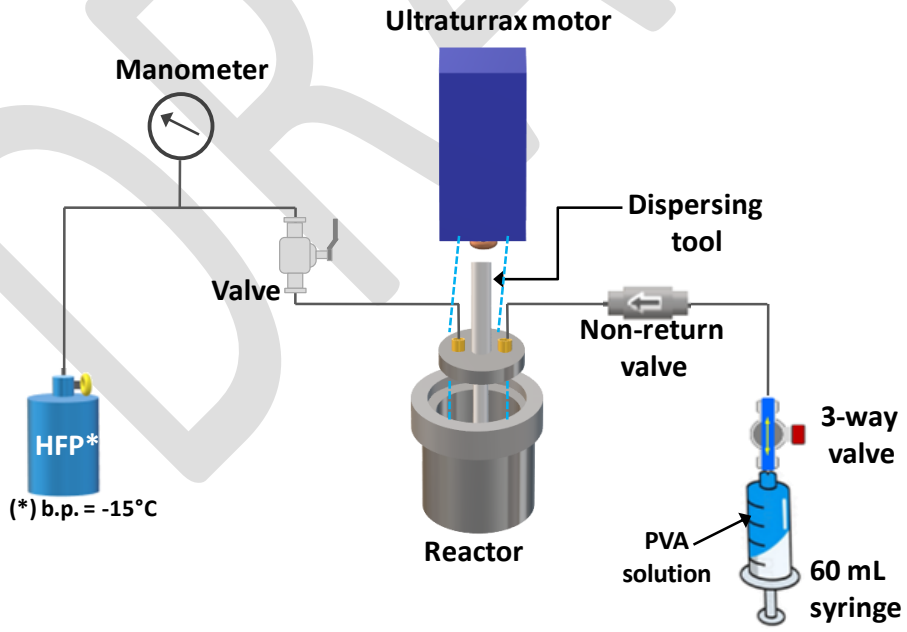

Scheme 1. Reaction setup for PVA-HFP nanodroplets formulation

2.2.3. Size distribution determination and stability of nanodroplets

The size distribution of PVA/PFB nanodroplets is determined at RT by dynamic light scattering (DLS). The suspension is diluted 100 fold (V=1 ml) and placed into a cylindrical quartz cuvette. Measurements are carried out at 90° using a photometer equipped with a BI-200SM goniometer, a BI-9000AT (Brookhaven Instruments Co.) correlation board and a solid state laser source emitting at 532 nm. Analysis of the autocorrelation function, g_2 (q, t), of the scattered intensity was carried out using the cumulants algorithm provided as part of the standard software package of the instrument. The stability of the nanodroplets is followed by re-measuring their size distribution over time (up to 15 days).

2.2.4. Microscopy study of acoustically activated nanodroplets

An overall observation of the nanodroplets samples, before and after their conversion to microbubbles, is carried out using an inverted Eclipse model Ti-E microscope (Nikon Instruments, Japan) equipped with a 40× long-working distance objective (S plan Fluor ELWD 40× Ph2 ADM). The ADV activation is performed using an SP100 sonoporator (1 MHz) from SONIDEL (Dublin, IE). Typically, 200 µl of the PVA/PFB/HFP nanodroplets are filled into an "Ibidi" microchannel slide (50 mm × 5 mm × 0.4 mm) (Germany) and fixed in a degassed water tank, heated at 37°C and placed on the microscope. The sonoporator probe is immersed in the water at 2 cm height. Acoustic vaporization is carried out at 1MHz central frequency and 100% duty cycle for 30s by applying an US power of 2W/cm^2. The transition NDs → MBs upon core vaporization is followed by bright field microscopy (40×) before and after the ultrasound exposure. For these experiments the droplets in the microchannel were 20 fold diluted in human serum.

2.2.5. Acoustic attenuation measurements

The experimental setup is described in Scheme S1 in the Supplementary Material. A volume of 200 µl of nanodroplets bulk suspension are introduced into a glass cell (2cm×2cm×4cm) containing degassed DMEM. The latter features two openings at opposite sides separated by a distance of 2 cm allowing contact with the emitting and receiving flat transducers (10 MHz, Olympus V311). A waveform generator producing consecutive sinusoidal ultrasound bursts at frequencies ranging from 0.5 to 20 MHz (in steps of 0.25 MHz) is used. A constant input voltage of 6 V was applied at each frequency, resulting in acoustic pressure levels below 60 kPa. The attenuation was deduced from the transmitted signals detected by the receiver by means of a reference method, where the reference is the DMEM medium. The acoustic attenuation measurements of both PVA/PFB and PVA/HFP nanodroplets are performed before and after

ADV. For activation the nanodroplets are exposed to ultrasound (duty cycle 100, 0.1–3.6 W/cm^2, 30 s) using the sonoporator described in section 2.2.4.

2.2.6. Temperature-induced Spontaneous Vaporization of PVA/PFB NDs by DSC:

Temperature activation of PVA/PFB NDS was examined using a TA Q2000 differential scanning calorimeter (TA Instruments, MI, Italy). 30 µl of PVA/PFB NDs pellet were filled into an aluminum pan then sealed using a hermetic aluminium lid. The scan was performed from 10 to 110 °C at a heating rate of 3°C/min and under a nitrogen flow of 50 mL/min.

2.2.7. Tissue-mimicking phantoms preparation

Poly(acrylamide) hydrogels (PAM) is synthesized as tissue-mimicking phantom material, starting from an aqueous stock solution of monomer, AM, and crosslinking agent, BIS, with a molar ratio AM/BIS equal to 29/1 (mol:mol) and AM concentration of 30% (w/v). The final concentration of AM in the phantom is diluted to 5% (w/v). In brief, 6.5 ml of AM stock solution, 32.5 ml of mQ water and 1 ml of APS at a concentration 8.5% (w/v) are mixed together and degassed for 5 min in an ultrasound bath cleaner. The resulting solution is cooled in ice for 5 min and transferred to the phantom can. Subsequently, 200 µl of PVA/PFB or PVA/HFP nanodroplets bulk suspension and 50 µl of TEMED are added. The mixture is stirred gently with a spatula to homogenously disperse the nanodroplets and is left at RT for 20-30 minutes to allow for the crosslinking (See Scheme 2a).

In another experiment, the nanodroplets are entrapped in an ultrasound gel (see details in the Supporting Information section 1.1).

2.2.8. Photon irradiation protocol

Preliminary X-ray radiation experiments were performed at room temperature. Triplicated tissue-mimicking phantoms of PVA/PFB or PVA/HFP nanodroplets were brought to the radiotherapy room and fixed in a water tank holder located at isocenter (see **Scheme 2b** in the Supporting Information). The radiation beam was delivered by a linear accelerator (Elekta Precise®) with 6 MVor 15 MV photons within a field size of 20×20 cm^2. PVA/PFB NDs were irradiated, at a dose rate of 5 Gy/min, with a cumulative total dose ranging between 2-10 Gy. Negative control experiments were performed on non-irradiated nanodroplets phantoms being incubated for 5 min at RT in the water tank, as well as on pure PAM phantom, i.e. without the nanodroplets, being delivered a 10 Gy dose. In order to assess the radiation effect on the PVA/PFB and on PVA/HFP nanodroplets, the phantoms were imaged pre- and post-exposure to radiation usinga clinical US apparatus (Mindray DP50, Milan) equipped with a linear transducer (f_c 7.5 MHz). Each phantom was scanned by taking 3 independent images to cover the entire surface as illustrated in **Scheme**

2c of the Supporting Information. All the images were acquired at the same gain and under a low mechanical index value of 0.1 in order to prevent NDs acoustic vaporization induction during US inspection.

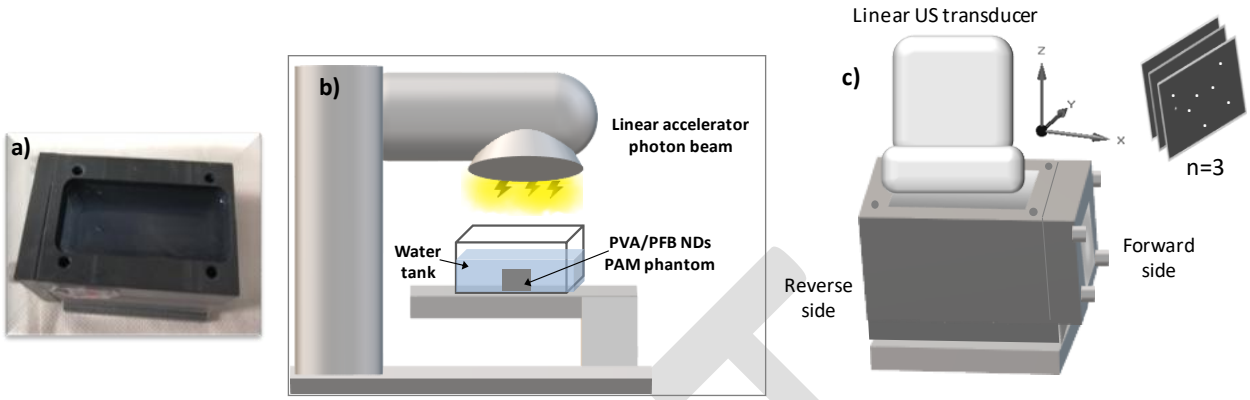

Scheme 2.a) Photograph of PAM hydrogel phantom incorporating PVA/PFB NDs, b) Schematic of the photon beam irradiation setup for PVA NDs phantoms, c) Illustration of an ultrasound imaging scan of the phantom through Y axis using a linear transducer.

2.2.9. Proton irradiation protocol

Proton irradiation studies were carried within the research facility of the Centre de Resources du Cyclotron (UCLouvain, Louvain-la-Neuve, Belgium), following the protocol described by (Carlier et al., 2020): The cyclotron (CYCLONE 110) produces a mono-energetic, passively scattered proton beam at 62 MeV. The proton range was modulated in discrete steps by inserting different thicknesses of degrader material in front of the irradiated sample. A brass aperture of 40 mm diameter was positioned in front of the phantoms to define the field size. The phantoms (as described in section 2.2.8/Scheme 2a) were fixed in a thermalized water tank (KU Leuven, Belgium) at 25°C, equipped with an immersed thermocouple (accuracy: ±0.5°C) and bearing a 3 mm entrance window. In this experiment, we addressed the PVA/PFB nanodroplets, with the aim to compare the effect of the beam features on the sensitivity response of these NDs type. The phantoms were irradiated under a proton flux of $7.92 \cdot 10^6$ protons/(cm^2 s), from the forward side with an equivalent 10 Gy fluence of $1.19 \cdot 10^9$ protons/cm^2 and from the reverse side with a fluence of $2.38 \cdot 10^8$ protons/cm^2, i.e. equivalent to 2 Gy dose. (see representative Scheme S2 in the Supporting Information)

2.2.10. Image processing

All the images recorded with the US imaging system were analyzed off-line using ImageJ freeware (Schindelin, 2012). ROIs with dimension of (30×23 mm) covering the scan zones of each phantom, i.e. 3 frames per phantom, were selected. The bubbles from the pre- and post-radiation images were counted by the software based on the pixel grey value threshold with respect to the

background, i.e. being considered as maxima. The results are presented as an apparent microbubble count, where speckles were assumed to be originated from a single bubble with an average position coincident with its center, even though signal from multiple microbubbles might be detected in the same spot zone (Viessmann et al., 2013).

The statistical data were calculated as mean ± standard deviation of bubbles count between irradiated/un-irradiated triple phantoms, treated at the same conditions, and by considering the three ROIs for each phantom.

When a high US contrast signal is generated due to high bubbles density, an average grey value in the selected ROI was measured using Image J default threshold profile function: e.g. for the experiments performed in ultrasound gel phantoms (details in Section 1.1. of the Supporting Information) in which the droplets were not homogenously dispersed but accumulated in a dense spot, as well as for ADV tests.

RESULTS AND DISCUSSION

3.1. Poly(vinyl-alcohol) nanodroplets formulation

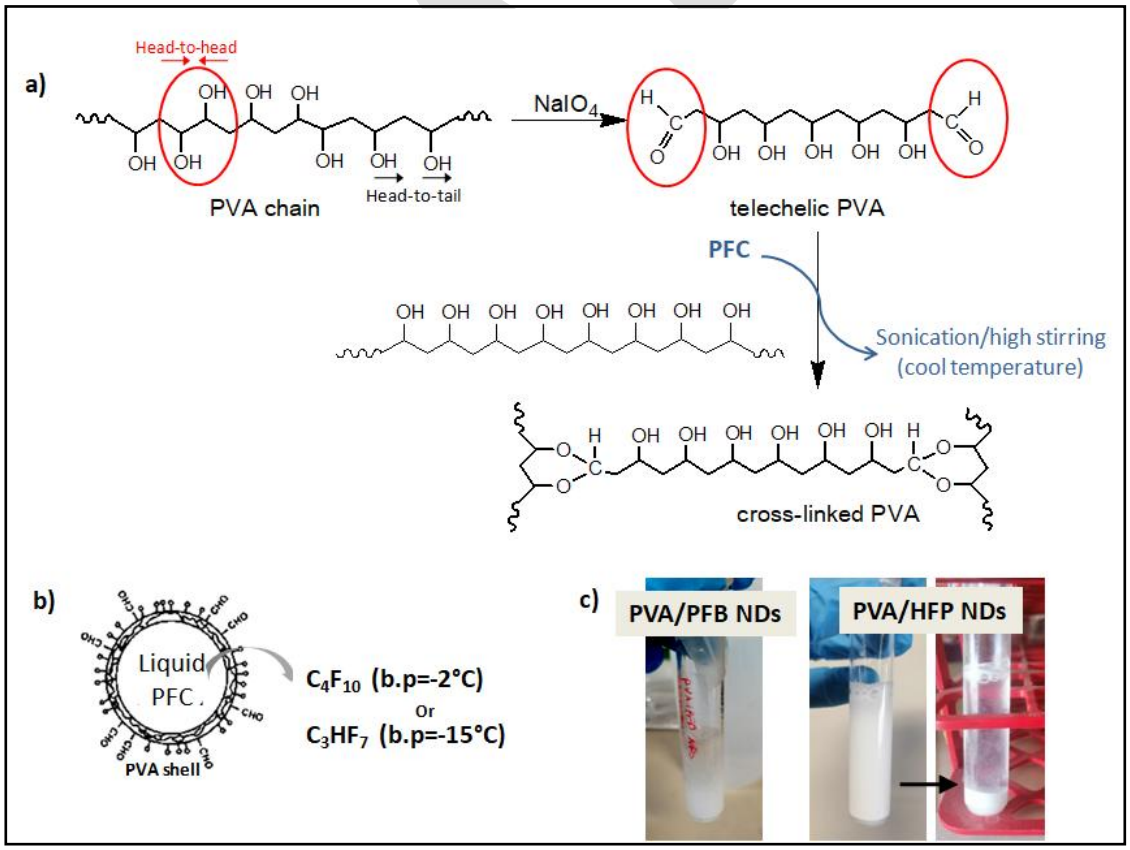

Scheme 3. a) Chemical reaction scheme of PVA shell crosslinking during PFB/HFP encapsulation, b) structural representation of PVA shelled nanodroplets, and c) photographs of yielded PVA/PFB and PVA/HFP nanodroplets (NDs tend to sink due to PFC higher density than water).

PVA is a biocompatible polymer very often used in the preparation of micro/nanoemulsions for diverse biomedical applications from drug delivery to multimodal imaging. In particular, the preparation of crosslinked air filled PVA microbubbles for ultrasound imaging was reported in the past literature by numerous studies (Cavalieri et al., 2005; Chen et al., 2020; Sirsi and Borden, 2009). Herein, we take advantage of the knowledge on the formulation of PVA MBs and we apply the same chemistry to the development of PVA nanodroplet shells encapsulating a liquid perfluorobutane core (C_4F_{10}, b.p. -2°C). In order to obtain droplets emulsions from PFCs in the gas state at room temperature and atmospheric pressure, these latter must be liquefied under pressure, at low temperature or both. The first encapsulated PFB droplets formulation was obtained by Sheeran *et al*, derived by condensing under a pressure of 170 kPa a cooled suspension of commercial lipid shelled microbubbles, known as Micro-Marker (VisualSonics, Canada) (Sheeran et al., 2017). In this work, PFB is directly confined in the liquid state, following the procedure described previously and based on a former condensation in liquid nitrogen (Toumia et al., 2019). A milky suspension of high yield sub-micron droplets is obtained by sonicating a mixture of a few microlitter large PFB liquid droplet and telechelic PVA solution. During the sonication process, a fraction of PFB vaporizes and fills the head space of the sealed vial, increasing therefore the internal pressure. The remains of liquid PFB divide into tiny submicron drops being englobed with PVA. The crosslinking of the shell occurs between the acetalization of aldehyde groups derived from the previous splitting reaction of the polymer chains with periodate (see **Scheme 3a**). This reaction leads to a viscoelastic and robust shell for an enhanced stability of nanodroplets in their metastable state. In addition, the un-reacted aldehydes and hydroxyl moieties on the surface confers to the system a good chemical versatility for further functionalization, e.g. by fluorescent dyes labelling, anti-cancer drugs, targeting antibody/peptides, nanoparticles, etc, towards a multimodal agent for theranostics and dosimetry (see Figure S1 in the Supporting Information) (ref). The same approach yields high concentrations of PVA/HFP NDs that can be obtained by changing the gas core to be liquefied (see Scheme 3b). The droplets remain stable as stored in sealed vials; however, exposure to environmental pressure induces a striking spontaneous vaporization difficult to control. Therefore, HFP based NDS will be considered in this study only for comparison sake with respect to the radiation response. At the current stage, more effort is needed in order to optimize their stability for envisaging their use possibly as injectable devices.

3.2.Temperature-induced Spontaneous Vaporization of PVA/PFB NDs

The NDs are designed to allow for an enhanced life-time stability with respect to common thin lipid shelled low b.p PFC droplets, and to be resistant against spontaneous vaporization not only at

physiological temperatures but also under extreme heating, e.g. for the estimation of the contribution of temperature to NDs interactions with ionizing radiation according the thermal spike theory predictions (Seitz, 1958). The polymeric encapsulation of low b.p PFCs has been already suggested to provide an alternative route for increasing the Laplace pressure and thus the half-life of NDs. For perfluorbutane, some studies used the shell crosslinking by UV exposure either by building triblock copolymers or conjugating a thin diacetylene monomers (Huang et al., 2017; Park et al., 2012; Toumia et al., 2019). Regardless the shell type, the additional Laplace pressure is imposed upon the core interior because of the curvature and interfacial energy (see equation 2) and contributes in stabilizing the droplets by increasing the boiling temperature of perfluorocarbon.

$$\Delta P = P_{in} - P_{out} = \frac{2\sigma}{r} \qquad (2)$$

Where P_{in} and P_{out} are the pressures inside and outside of the nanodroplet particle, σ is the surface tension of the shell and r is the radius of the droplet.

Generally, vaporizing a nanodroplet into a microbubble requires energy to be brought to the system in order to overcome the nucleation barrier within the superheated liquid. However, exposing the droplets to temperatures beyond the superheat limit of the liquid core induces their spontaneous vaporization without ultrasound, optical or charged particle radiation stimuli. We have analyzed, at atmospheric pressure, the temperature effect on the vaporization of the obtained PVA/PFB droplets by performing a DSC scan (see Figure 1). The complexity of the thermogram, which reveals several minor peaks in the temperature scan range (30°C-70°C), is related to vaporization of few unstable nanodroplets either due to larger size or thinner shells. However, the major vaporization of PFB droplets stabilized with the crosslinked PVA shell occurs at a temperature of 78°C. The Application of Antoine's parameters, for uncoated PFB, predicts a rise of the boiling temperature to about 60°C when the external pressure corresponding to its vapour at room temperature is equal to 3.4 atm. Sheeran *et.al.* demonstrated, based on Antoine's equation, that decafluorobutane is promising for obtaining metastable droplets above the body temperature when particle diameters are the range of 100-700 nm, suggesting the potential of its encapsulation to remain stable owing to the increased surface tension effect (Sheeran et al., 2011a). This behaviour nearly applies to sub-micron perfluorobutane nanodroplets with a thin monolayer shell of PCDA (see Figure S2 in the Supporting Information for comparison). Several theoretical models assume that the shell features in terms of viscosity and elasticity affect the induced shift of the phase transition temperature, and therefore any change in shells composition may result in higher or lower droplet stability. For example, Mountford and Borden reported a considerably

high vaporization shift up to 74°C for submicron PFB droplets with a lipid shell (Mountford and Borden, 2016), in a good agreement with the temperature of superheat limit value, calculated for PFB according to empirical model (equation 2) and estimated to 73°C (see Table S1 in the Supporting Information). The significant and remarkable increase of liquid→vapour transition in the case of PVA/PFB NDs, i.e. 78°C, could be attributed to an additional work sufficient to extend the PVA crosslinked chains as suggested by Church's theory on thick polymer shells (Capece et al., 2016; Church, 1995).

\

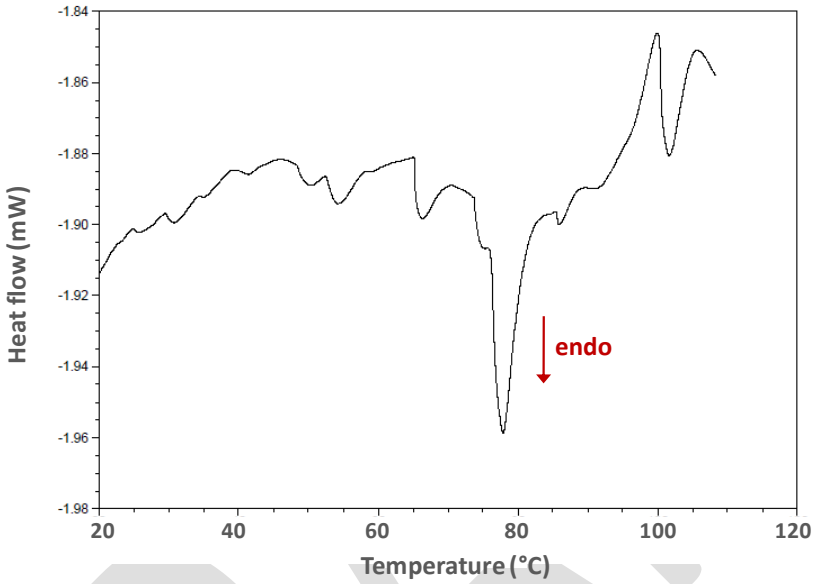

Figure 1. Differential scanning calorimetry thermogram of PVA/PFB nandroplets. Exothermic heat: up

3.3. Nanodroplets Size Distribution

In general, the size distribution of nano/micro-emulsions, prepared by a sonication process, is conditioned by the contribution of many factors. These include volume ratio between the different phases, the shape of the container, sonication conditions, etc. Contrarily to microfluidic methodologies, or extruder technologies, ordinarily used with higher b.p. perfluorocarbons, the lack of control of all parameters often leads to a large size distribution. Hence, in agreement with other studies reporting on nanodroplets (Loskutova et al., 2019), PVA/PFB NDs exhibit a polydisperse size distribution with an average diameter of 700 nm (see inset in Figure 2a). Polydispersity can be overcome by extracting different sub-populations of nanodroplets using selective centrifugation (see Figure S3a-b in SI) to narrow the size distribution. However, the shelf life evolution study of size-sorted nanodroplets shows that, within three weeks, either the larger and tinier sub-populations keep relatively a stable size (Figure S3c of the Supporting Information). This is again due to the polymer thick shell resulting in enhancing the nanodroplets stability against coalescence or partial vaporization over time. Yet, in this work we will mainly focus on the interaction of NDs with radiation without taking into consideration size restrictions.

Accordingly, all experiments discussed herein were performed on bulk PVA/PFC suspensions. Furthermore, it is to mention that the role of the crosslinks in stabilizing the nanodroplets clearly emerges when size and number of particles with and without oxidation of PVA are compared. Besides being highly irreproducible, the PFB nandroplets encapsulated in a non-crosslinked PVA shell result dramatically unstable over a short time. The crosslinks are expected to increase the elastic modulus of the shell and to allow for limiting the diffusion of the PFC core throughout the interface, preventing droplets expansion and vaporization.

3.4. Nanodroplets phase transition by acoustic activation

The nanodroplet→microbubble conversion was primarily characterized using bright field microscopy and by triggering an acoustic droplet vaporization process, in order to assess the increase shift of the size distribution. Prior to their vaporization, both PVA/PFB and PVA/HFP NDs appear as tiny spots, limited by the microscope resolution. The size of PVA/PFB NDs almost increased by a factor of 10 upon their activation at 1 MHz, yielding microbubbles with an average size compatible with blood capillaries diameters, i.e. of 6.6 ± 1.9 μm. The size growth factor is considerably lower as compared to a recent study on PFB NDs encapsulated in a thin crosslinked lipid shell, i.e. PCDA, and simulating the same emulsifying conditions. In the latter case, the resulting MBs increased by a factor of 30 respect to the initial droplets size. On the basis of the ideal gas behavior, it is often reported that ADV promotes the core expansion of about 5- to 6-fold over a millisecond time lapse for lipid shelled PFC droplets (Mountford and Borden, 2016; Sheeran et al., 2017, 2012). However, as far as the microbubbles size is concerned,the ADV process leading to MBs production is not yet completely elucidated as it derives from a complex contribution of several factors, such as medium, perfluorocarbon density, shell type; uptake of gases from the air-saturated host medium etc. (Kripfgans et al., 2000). In addition, the acquisition time is a factor to take into account in analyzing NDs → MBs transition growth. The instantaneous capture of a 400 nm sized droplet expanding into a microbubble of 1.4 μm diameter was reported by Reznik *et.al.* within a time lapse of 1-1000 ms from ADV (Reznik et al., 2011). Furthermore, a major increase (about 25 times) of the particle diameter after ADV has been reported for lipidic droplets of perfluoropentane core suspended in saline containing bovine serum albumin. Indeed, once vaporized, the bubbles nearly coincide with theoretical expansion predictions on a microsecond timescale, although this may differ if bubbles are monitored for longer times. Moreover, several *in vitro* studies have shown that bubbles may expand beyond the ideal gas law predictions due to the influx of dissolved gases present in the surrounding media (Sheeran et al., 2013a, 2011b). As for samples having a core made of lower b.p than PFB one, i.e. HFP, the phase transition of PVA/HFP NDs resulted in slightly larger microbubbles with an

average diameter of 8µm. In a similar way, the nanodroplets are observed as tiny spots by light microscopy prior to their activation. However, the growth factor could not be estimated at this stage, due to the instability of the encapsulated HFP droplets during a DLS measurement. These results, as illustrated in **Figure 2a-b/d-e**, confirm that PVA/PFB could be used in the future studies for intravenous injection, nonetheless HFP NDs could not represent a good candidate for *in vivo* applications at the current stage due to their unhandled stability when exposed to ambient pressure, but will be considered in the study only in terms of radiation response comparison with PFB counterparts.

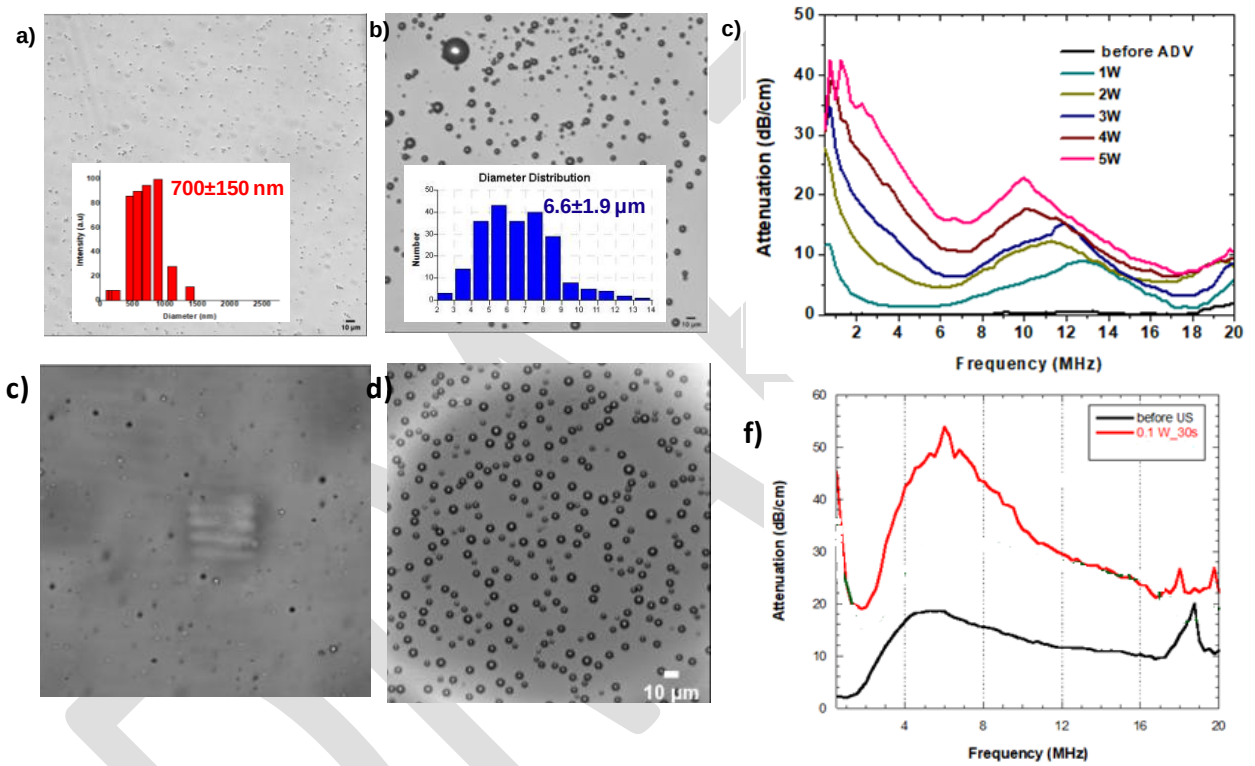

Figure 2. Acoustic activation of PVA nanodroplets: a) and b) bright field microscopy images of PVA/PFB respectively before and after ADV (1 MHz, 2W/cm^2, 30s); c) acoustic attenuation spectra of PVA/PFB after US activation with increased applied intensity; d) and e) bright field microscopy images of PVA/HFP respectively before and after ADV (1 MHz, 0.1W/cm^2, 30s); f) acoustic attenuation spectraof PVA/HFP before and after US exposure.

Once more and similar to the previous experiment above, we have used a 1 MHz ultrasound sonoporator as an activation tool for the assessment of the acoustic attenuation properties of obtained microbubbles upon phase transition. The ADV threshold of nanodroplets is generally measured at frequencies in the MHz range, relevant for clinical ultrasound imaging. Additionally, besides the degree of superheat of the droplets core, other factors come into play such as size and shell effects, i.e. thickness and visco-elastic properties (Lacour et al., 2018). Figure 2c shows the resulting attenuation spectra of PVA/PFB NDs, before and after ultrasound exposure under

various intensities. The nanodroplets exhibit no acoustic attenuation before ultrasound exposure, i.e. when the core is in a liquid state. Subsequently, elevating gradually the applied ultrasound intensity (up to 5W/cm^2) yielded to the concentration rise of converted microbubbles, which is translated by a proportional increase of the acoustic attenuation with an activation threshold of 1W/cm^2. Moreover, we notice that the attenuation spectra of PVA/PFB MBs display two resonance frequency components, i.e. at 1 MHz and at 10 MHz. The difficulty in identifying resonance frequency peak and the band width, typically associated with damping mechanisms, is often reported for polydisperse microbubble dispersions (Parrales et al., 2014). It is well known that as droplet size diminishes, the expansion factor will theoretically be dominated by the effect of surface tension/Laplace pressure, while the expansion factor for very large droplets (negligible Laplace pressure) becomes dominated by ambient pressure leading, respectively, to higher or lower acoustic resonance frequency. Though, we exclude that the observed acoustic behaviour could be size related. In fact, the sub-populations of nanodroplets with a significant average size lag, i.e. 400 nm and 1.5µm, exhibit similar acoustic spectral features to the droplets activated from bulk suspension (see **Figure S4** of the Supporting Information). As the second peak occurs at 10 MHz, in agreement with air filled PVA microbubbles (Domenici et al., 2019), we suggest that the lower frequency (i.e. 1MHz) could be attributed to the resonance of the microbubbles, while the higher frequency to their inertial cavitation, respectively: commonly, it is expected that oscillation amplitudes of a gas bubble will be amplified significantly if the excitation frequency of impinging ultrasound closes to the resonance (or the main resonance) or higher harmonic resonances, typically the second resonance frequency (Versluis et al., 2020).

Contrarily to PFB NDs, the PVA/HFP NDs show a significant attenuation prior to US exposure due to the unstability and spontaneous transition of nanodroplets to microbubbles. In fact, the resistant PVA/HFP NDs are easily activated at low intensity, i.e. 0.1 W/cm^2 (see Figure 1d), due to the very low b.p. (-15 °C) of the liquid core. A sharp attenuation is observed at 0.5 MHz followed by a large frequency resonance band at 6 MHz characterizing the attenuation spectra. This can be explained as HFP NDs featuring different shell parameters in terms of crosslinking efficiency and visco-elasticity resulting from the use of an ultra-dispersing tool during the preparation process.

3.5. Nanodroplets fixation in tissue-mimicking phantoms

The tissue-mimicking phantoms were used as means to stably support the droplets at either room or higher temperature conditions, e.g. 37°C, with a minimized induced spontaneous vaporization. Two phantoms were mainly tested in this study (i.e. polyacrylamide (PAM) hydrogel and

commercial ultrasound gel ®), where NDs could be incorporated while at RT. The phantoms were optimized based on their thermal stability at 37°C to fit with future *in-vivo* purposes, in addition to the ability of NDs to expand into microbubbles when exposed to a stimulus such as ultrasound. The background signal of the phantom was first assessed by US imaging (f_c=7.5 MHz) at a low mechanical index (MI =0.1) to avoid any NDs acoustic activation. Contrarily to microbubbles which are strongly reflective due to the gaseous core, below the acoustic threshold, nanodroplets are invisible to ultrasound imaging due to their small size and similar impedance to tissue (Mannaris et al., 2020). Figure 3a and Figure S5 in the Supporting Information, show that PVA/PFB NDs present an almost empty background at room temperature and after heating at 37°C, with a limited number of bubbles resulting from spontaneous vaporization during phantom preparation or incubation. Moreover, we have evaluated the acoustic vaporization threshold of PVA/PFB NDs in the phantoms by increasing the transmit power of the probe and consequently the mechanical index. Such parameter is determinant in order to avoid vaporization interferences induced by ultrasound during the imaging of the droplets phantoms for the detection of ionizing radiation response. Haung et.al reported on crosslinked triblock copolymer NDs affording greater PFB emulsion stability and requiring higher mechanical index with respect to non-crosslinked emulsions (Huang et al., 2017). In agreement, the vaporization thresholds of PVA/PFB NDs begin to occur at a mechanical index of 0.4 (see Figure 3c and Figure S6 at the supporting Information), suggesting that all images should be acquired below a MI = 0.4, while activation threshold for thin lipid shell counterparts, i.e poly(PCDA,) is relatively lower (see Figure S7 in the Supporting Information).

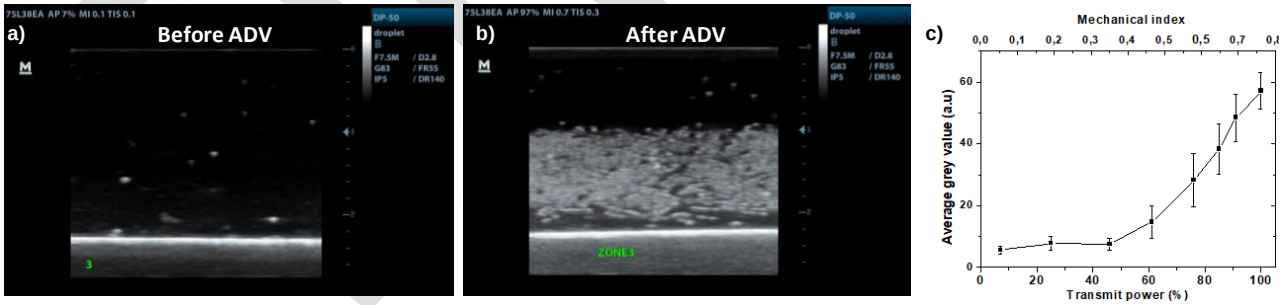

Figure3. *In vitro* US activation of PVA/PFB nanodroplets in PAM tissue-mimicking phantom: US image of the phantom before ADV a) and b) after ADV (MI= 0.7); c) activation trend of the nanodroplets illustrating the calculated average grey value of acquired US images as a function of applied mechanical index/transmit power.

3.6.X-ray radiation response of nanodroplets

The nanodroplets phantoms prepared according to the protocol described in section 2.2.8, were exposed to a clinical X-ray photon beam. The potential of a dosimetric response of the superheated PVA/PFB and PVA/HFP NDs is assessed by quantifying the increase of contrast

generation in the ultrasound imaging, which correspond to the nanodroplets vaporized during radiation. The apparent bubbles count along the X-ray beam path was derived from the acquired ultrasound images, as illustrated in Figure S8, by detecting each single bright pixel spot at the ROI in the depth direction and the lateral length of the phantom. The counts from the full phantom scan views were combined and divided by the number of frames/scan (n=3) in order to prevent loss of profile information. All bubbles from triplicate independent phantoms were summed and averaged in to ensure fair statistics and attenuate fluctuations. **Figure 4a-d** displays US images of PVA/PFB NDs as dispersed in PAM phantom prior and after irradiation at RT with cumulative doses between 2-10 Gy and under beam energy of 6 MV. The background signal present in the phantoms before irradiation (see Figure 4a) was due to a certain amount of bubbles introduced upon injection or to spontaneous vaporization of a small fraction of nanodroplets during phantom preparation. The increase in bubble count was fairly higher after receiving total radiation doses of 2, 5, and 10 Gy. Besides, the control phantoms, i.e. equally prepared but not being irradiated (see Experimental Section 2.2.7), show an almost constant bubbles count before and after their incubation in the water tank at RT, simulating the same conditions of the irradiated ones (see Figure S9 in the Supporting Information). This confirms that the increase in US contrast signals post-radiation results from the interaction of droplets with X-rays beam and is not a time induced effect. Moreover, we verified the radiation response of the PAM hydrogel matrix in terms of ultrasound contrast generation. As illustrated in Figure S10 in the Supporting Information, the pure PAM phantom, i.e. without nanodroplets, resulted in a background-free ultrasound image after irradiation, demonstrating that the ionizing radiation-induced contrast generation was only attributed to the presence of nanodroplets that vaporized. However, the PVA/PFB NDs as concentrated in a single compact area in the US gel matrix reveal a more significant response to X-ray at RT. In this case, the quantified average grey contrast signals from the recorded post-radiation US images increased by a factor of 3 fold as compared to pre-radiation images (see **Figure 5 a-c**). Yet, we do not consider commercial US phantoms as an accurate matrix for the study, since it is difficult to avoid the introduction of bubbles artifacts during the injection of nanodroplets and therefore to reproducing phantoms, relatively, with the same ROI and same background.

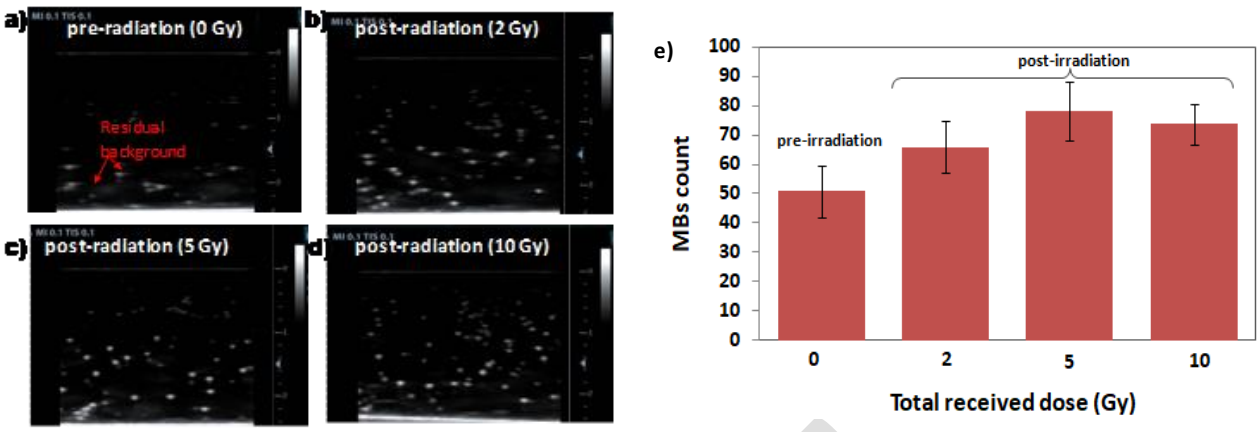

Figure 4. US images of PAM phantom with dispersed PVA/PFB nanodroplets irradiated with cumulative photon dose at a rate of 5 Gy/min and 6 MV beam energy: a) pre- X-ray exposure (i.e. 0Gy), b) post 2 Gy, c) post 5 Gy and d) post 10 Gy. e) Statiscal bubbles count on post-processed US images scans of irradiated phantoms (×3) using Image J freeware.

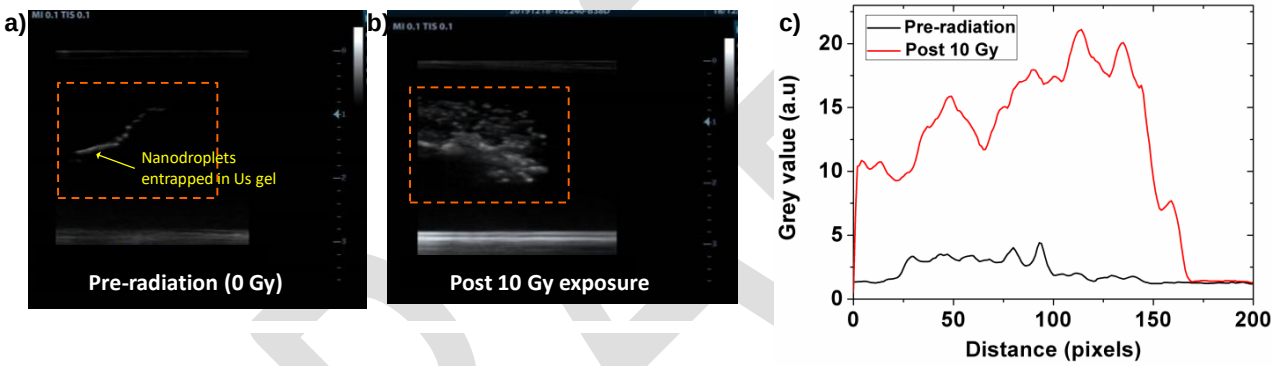

Figure 5. PVA/PFB nanodroplets entrapped in ultrasound gel®: a) US image of phantom before photon irradiation and b) US image of phantom after 10 Gy photon exposure at a rate of 5 Gy/min and 6 MV energy; c) grey average analyses profile spectra of the selected ROI from US images pre-and post-10 Gy X-ray exposure. The dashed square indicates the selected ROI.

As far as we know, little is known on the sensitivity of phase change NDs due to X-ray ionizing radiation. All the same, a previous study demonstrated that, unexpectedly, some commercialized microbubbles were subjected to a change in their acoustic attenuation features when exposed to radiotherapeutic beams. e.g. X-ray (Verboven et al., 2014). Nonetheless, the physics behind this modification was not clear. Contrarily to microbubbles, the nanodroplets herein would rather act as an acoustic off/on switch with their response to ultrasound interrogation going from 0 (in the droplet state) to 1 (in the gas state). The mechanism behind droplet vaporization, in this case, is yet to investigate, though we believe that many factors besides the delivered dose could take part in radiation sensitivity. These include beam energy, shell thickness, temperature and degree of superheat of the PFC core, recoil sub-products, etc. For this reason, we evaluated the response of PVA shelled NDs under different conditions by testing the dose effect as well as operating beam

energy, and last but not least by increasing the degree of superheat with a lower boiling point PFC, i.e. HFP (-15°C). **Table 1** summarizes the results of ultrasound contrast enhancement from PVA/PFB and /HFP NDs, pre-and post-X ray radiation at the same delivered doses, and the tested different conditions, i.e. temperature or beam's energy. The percentage of vaporization detection was calculated as follows in eq. 3:

$$\frac{MBs\ count_{post-rad} - MBs\ count_{pre-rad}}{MBs\ count_{pre-rad}} \times 100 \qquad (3)$$

It was observed, that, at 25°C, increasing the beam energy to 15 MV did not amplify the response of the nanodroplets and resulted in a similar enhancement obtained with 6 MV energy, within the error range (see also Figure 6). As a matter of fact, the X-ray photons produce a maximal LET of 25 KeV/µm, therefore, PFB is not theoretically prone to undergo a phase transition upon irradiation at RT or even at body temperature because of the higher LET threshold required, i.e. 370 KeV/µm and 145 KeV/µm, respectively (D'Enrico, 2001); Heymans et al., 2020) (see Table S1 in the Supporting Information). This explains the low generated US contrast when it is compared with an acoustic activation. Nonetheless, the slight observed vaporization can be attributed to few NDs whose core has been partially vaporized prior to X-ray exposure during the transfer operations into the radiotherapy facility, leading to expanded droplet size with decreased curvature. Such phenomenon is due to the formation and continuous collapsing of vapour embryos in the core leading to the increase of PFB superheat degree close to its limit, and upon which a small perturbation (e.g. pressure, temperature increase, and radiation exposure) becomes sufficient to nucleate an adequate number of embryos and to induce a complete vaporization (Avedisian and Andres, 1978; Blander and Katz, 1975; Monde, 2015). Thus, close to their superheat degree limit, the nanodroplets require a lower density of energy deposition which eases their vaporization by X-ray. Similar findings were described with superheated emulsions for radiation dosimetry when increasing the temperature (D'Enrico, 2001). The superheat degree of PFB core should be increased up to 0.57 for most NDs in order to make them efficiently sensisitive to photon radiation and obtain a complete vaporization. This would require a temperature and/or an acoustic energy supply with the X-ray received dose to yield high US contrast signals as a result of massive droplet activation. The required temperature in such case should be raised above 60°C (see Figure S11 in the Supporting Information), making it unsuitable for *in vivo* purposes. On this basis, HFP (b.p =-15°C) was tested as alternative core aiming to reach X-ray sensitivity at physiological temperatures. In fact, due to the instability of PVA/HFP NDs and the difficult handling at ambient pressure leading to large spontaneous vaporization, the latter does not fit with theoretical predictions. The superheat degree of metastable liquid HFP is estimated equal to 0.35 and 045 at

RT and 37°C, respectively, requiring therefore higher LET threshold than X-ray photons for radiation-induced vaporization (Table S1 in the Supporting Information). However, Figure 7a-c shows a significant US contrast enhancement upon X-ray irradiation, which increased by a 3 fold factor after receiving a 10 Gy dose (Figure 7d). Moreover, Figure S12 in the Supporting Information clearly displays the foaming in an irradiated sample of PVA/HFP NDs with respect to un-irradiated control. Nevertheless, it is worth mentioning the low reproducibility of the phantoms incorporating HFP droplets due to the latter short life-time. The poor stability of PFCs with very low boiling points, remarkably inferior to 0°C, was claimed in numerous studies (Li et al., 2019). For example, sub-micron droplets with octafluoropropane (b.p. -36°C) obtained from the condensation of Definity microbubbles (Lantheus Medical Imaging, Inc., Billerica, MA, USA) were described by Sheeran *et.al.* (Sheeran et al., 2017). To our knowledge, HFP has not been reported in the literature as a core for phase-change contrast agents, and was suggested herein as intermediate between PFB and octafluoropropane. While droplets formulation was successfully obtained, the main challenge remains in achieving an enhanced stability allowing for easy handling and reproducibility of in vitro studies.

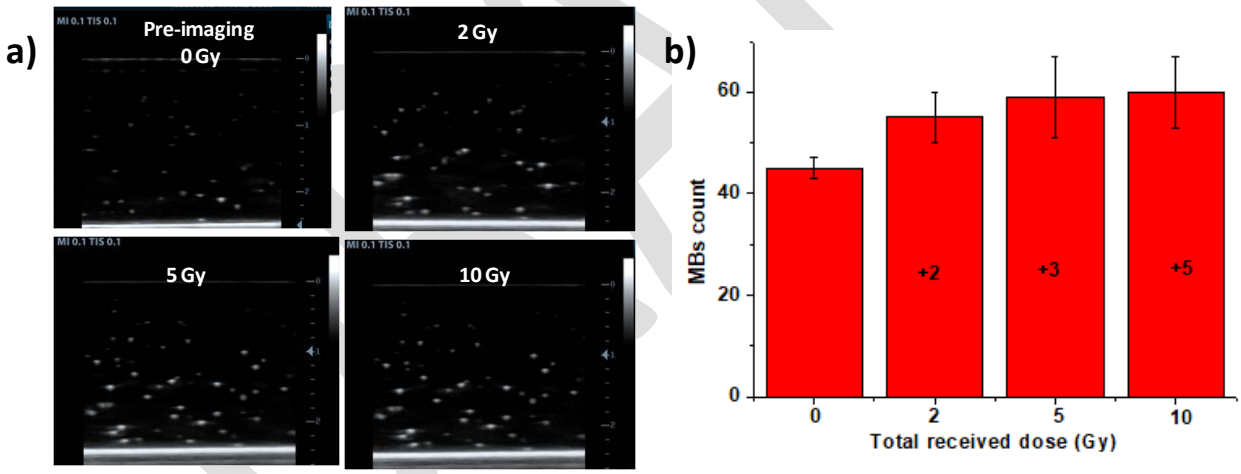

Figure 6.a) US images (MI= 0.1) of PAM phantom with dispersed PVA/PFB nanodroplets irradiated with cumulative photon dose at a rate of 5 Gy/min and 15 MV beam energy,b) Statiscal bubbles count on post-processed US images of the phantoms using Image J freeware.

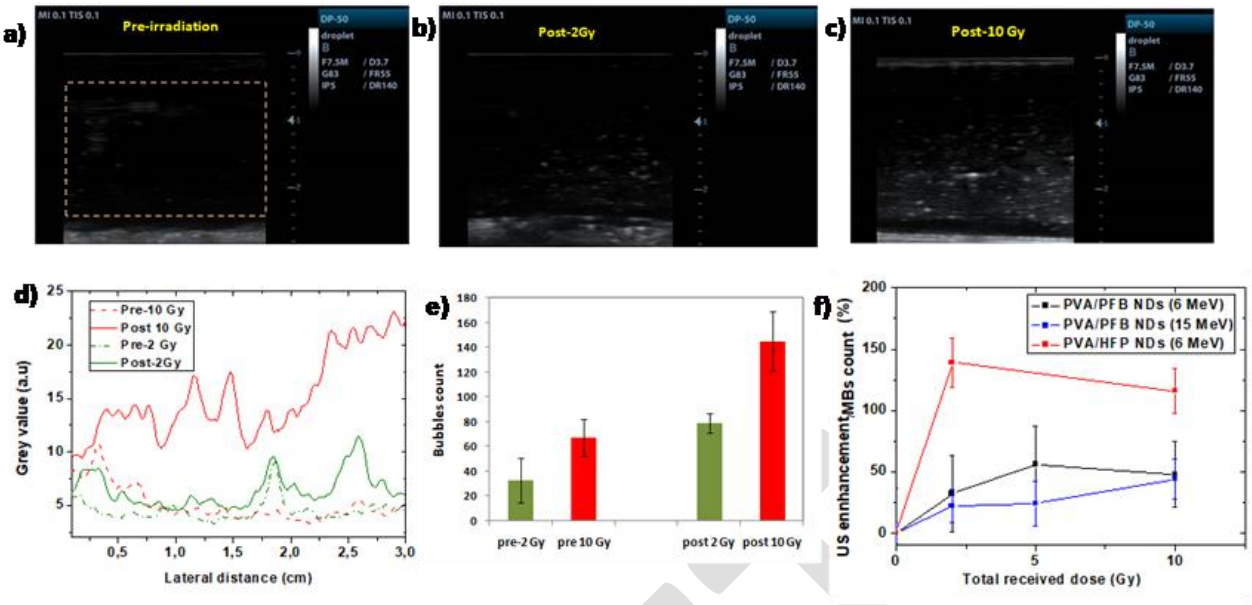

Figure 7. X-ray irradiation of PVA/HFP NDs in PAM phantoms at RT, under a dose rate of 5Gy/min and 6 MeV beam energy: a-c) US images (MI=0.1; f_c= 7.5 MHz) of pre-irradiation, i.e. 0 Gy, post- 2Gy and post 10-Gy, respectively. d) grey contrast value profile pre and post X-ray exposure; e) Statistical bubble count pre-and post-irradiation; f) US signal enhancement of PVA/PFB vs. PVA/HFP NDs as a function of received dose. The dashed square indicates the selected ROI.

Table 1.Summarizing results of X-ray induced vaporization of PVA shelled NDs

Core	Conditions	Pre-radiation MBs count	Post-radiation MBs count			enhancementof vaporization detection(%)		
			2 Gy	5 Gy	10 Gy	2 Gy	5 Gy	10 Gy
PFB	RT-6 MV	50 ± 9	66±9	78±10	74±7	32	56	48
	RT- 15 MV	45± 2	55± 5	59±8	60±7	22	24	44
	65°C-6 MV	93	-	-	>400	-	-	>300
HFP	RT-6 MV	33±18	79±8	-	-	139	-	-
		67±15	-	-	145±24	-	-	116

3.7. Comparison of PVA/PFB nandroplets response to primary proton beam radiation

The protons-induced vaporization of PFB droplets, coated with PVA or thin lipid PCDA shells, has been recently reported by our team aiming to proton range verification (Carlier et al., 2020) (Heymans et al., 2020). Although PVA/PFB NDs resulted in strong US enhancement and with promising range shift upon protons exposure at physiological temperature, it was demonstrated that the droplets were sensitive to recoil sub-products producing sufficient LET rather than primary protons. The purpose herein, relies only on comparing the behavior of PVA/PFB regarding the two types of radiation at the same conditions, i,e, temperature and delivered doses.

Figure 8a reports an US image of PVA/PFB in PAM phantom after being irradiated with a proton beam (see experimental section 2.2.10). The US probe was placed between the irradiated forward and reverse zones of the phantom container in a way to provide full coverage of the middle zone as well. Compared to X-ray photons, proton radiation shows a more efficient and significant droplets sensitivity at RT. The quantification of vaporized NDs upon exposure reveals an increase of detected bubbles in the background contrast signals from the irradiated reverse and forward zones respect to the non-irradiated middle zone used as a negative control. This increase has been quantified by 75% in the reverse position receiving 2 Gy dose and by over 300% in the forward zone which has received a total 10 Gy dose (see Figure 8b). The grey value profile plot of the entire frame (see Figure S9. in the Supporting Information) confirms the trend of MBs count histogram between forward, reverse and middle areas. Such enhancement result slightly lower than thin crosslinked lipid shell of PCDA, which yielded to an increase of US signals up to a factor of 5 under the same irradiation conditions (Carlier et al., 2020). The shell design for the coating of nanodroplets could affect their sensitivity, as the radiation can only affect the core from the outside through the shell thickness, and therefore would require a higher critical energy to be deposited for triggering the phase transition. This explains the difference observed between perfluorobutane nanodroplets with both shell types, though PVA NDs reveal to be more promising as an injectable dosimetric device due to their better durability. To this regard, Zacek et.al demonstrated that α radiation triggered complete phase transition of uncoated feron-12 droplets (b.p. -30°C) at a temperature above 35°C (Zacek, 1994).

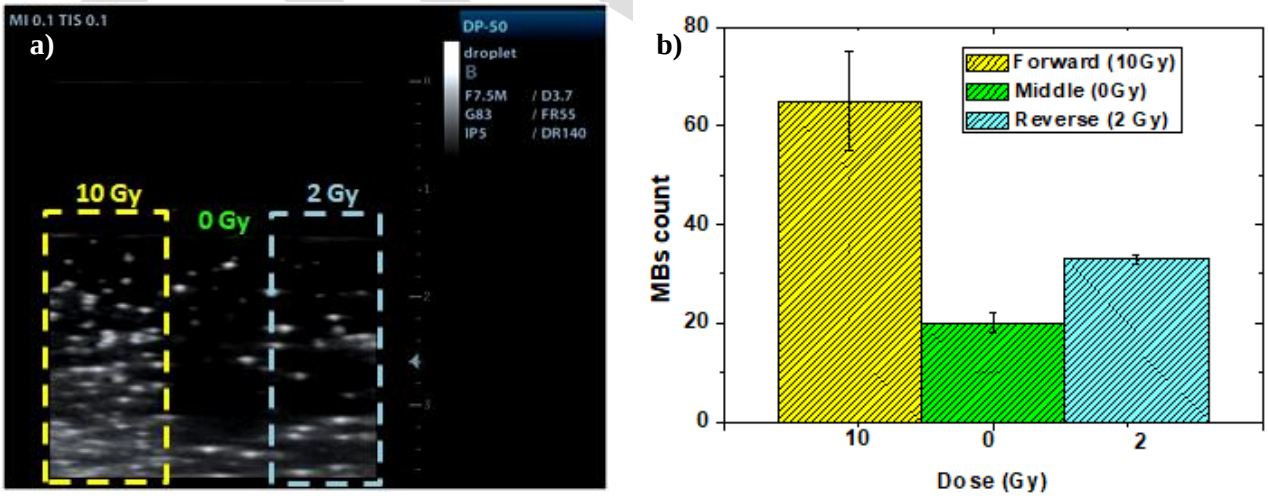

Figure 8. a) US image of PAM phantom with dispersed PVA/PFB nanodroplets partially irradiated at RTin forward zone with 10 Gy and in reverse zone with 2 Gy equivalent proton beam (62 MeV). The yellow and blue dashed squares highlight the irradiated ROIs, the images were acquired at 0.1 MI. b) Post-radiation microbubbles count diagram from forward and reverse zones as well as non-irradiated middle zone.

CONCLUSION

This study investigated the novel potentials of ultrasound imaging as a tool for radiotherapy dosimetry, by the means of injectable phase-change contrast agents viewed as modern bubble chamber detectors. The new formulation of PVA/PFB nandroplets, with a crosslinked shell, demonstrated an exceptional colloidal stability and good echogenicity. PFB nandroplets showed a moderate response to X-ray photons when entrapped in tissue-mimicking phantoms, suggesting that further efforts are needed in order to reach an optimal sensitivity. The unusual thermal stability of most PVA/PFB NDs at high temperatures above the physiological ones would play a key role in understanding the relation between radiation dose and temperature to induce vaporization. Radiation sensitivity of the nanodroplets is not strictly related to the shell type, although a slight difference in vaporization ease due to thickness and therefore to surface tension, but mostly to the degree of superheat of the liquid core and the ionizing radiation linear energy transfer. While preliminary results from PVA/HFP NDs to X-ray photons are promising in terms of US contrast generation upon X-ray exposure at clinical doses, future experiments will be addressing optimizing the stability of these latters.

REFERENCES

Amaldi, U., 1999. Cancer therapy with particle accelerators. Nucl. Phys. A, Proceedings of the International Nuclear Physics Conference 654, C375–C399. https://doi.org/10.1016/S0375-9474(99)00264-X

Apfel, R.E., 1998. Activatable infusable dispersions containing drops of a superheated liquid for methods of therapy and diagnosis - Abstract - Europe PMC. 5840276.

Archambault, L., Beddar, A.S., Gingras, L., Roy, R., Beaulieu, L., 2006. Measurement accuracy and Cerenkov removal for high performance, high spatial resolution scintillation dosimetry. Med. Phys. 33, 128–135. https://doi.org/10.1118/1.2138010

Avedisian, C.T., Andres, R.P., 1978. Bubble nucleation in superheated liquid—liquid emulsions. J. Colloid Interface Sci. 64, 438–453. https://doi.org/10.1016/0021-9797(78)90386-7

Barretta, P., Bordi, F., Rinaldi, C., Paradossi, G., 2000. A Dynamic Light Scattering Study of Hydrogels Based on Telechelic Poly(vinyl alcohol). J. Phys. Chem. B 104, 11019–11026. https://doi.org/10.1021/jp001863h

Beaulieu, L., Goulet, M., Archambault, L., Beddar, S., 2013. Current status of scintillation dosimetry for megavoltage beams. J. Phys. Conf. Ser. 444, 012013. https://doi.org/10.1088/1742-6596/444/1/012013

Blander, M., Katz, J.L., 1975. Bubble nucleation in liquids. AIChE J. 21, 833–848. https://doi.org/10.1002/aic.690210502

Bloemen-van Gurp, E.J., Mijnheer, B.J., Verschueren, T.A.M., Lambin, P., 2007. Total Body Irradiation, Toward Optimal Individual Delivery: Dose Evaluation With Metal Oxide Field Effect Transistors, Thermoluminescence Detectors, and a Treatment Planning System. Int. J. Radiat. Oncol. 69, 1297–1304. https://doi.org/10.1016/j.ijrobp.2007.07.2334

Brooks, C.L., Schietinger, A., Borisova, S.N., Kufer, P., Okon, M., Hirama, T., MacKenzie, C.R., Wang, L.-X., Schreiber, H., Evans, S.V., 2010. Antibody recognition of a unique tumor-specific

glycopeptide antigen. Proc. Natl. Acad. Sci. U. S. A. 107, 10056–10061. https://doi.org/10.1073/pnas.0915176107

Butson, M.J., Yu, P.K.N., Cheung, T., Metcalfe, P., 2003. Radiochromic film for medical radiation dosimetry. Mater. Sci. Eng. R Rep. 41, 61–120. https://doi.org/10.1016/S0927-796X(03)00034-2

Capece, S., Domenici, F., Brasili, F., Oddo, L., Cerroni, B., Bedini, A., Bordi, F., Chiessi, E., Paradossi, G., 2016. Complex interfaces in "phase-change" contrast agents. Phys. Chem. Chem. Phys. 18, 8378–8388. https://doi.org/10.1039/C5CP07538F

Carlier, B., Heymans, S.V., Nooijens, S., Toumia, Y., Ingram, M., Paradossi, G., D'Agostino, E., Himmelreich, U., D'hooge, J., Abeele, K.V.D., Sterpin, E., 2020. Proton range verification with ultrasound imaging using injectable radiation sensitive nanodroplets: a feasibility study. Phys. Med. Biol. 65, 065013. https://doi.org/10.1088/1361-6560/ab7506

Casolaro, P., Campajola, L., Breglio, G., Buontempo, S., Consales, M., Cusano, A., Cutolo, A., Di Capua, F., Fienga, F., Vaiano, P., 2019. Real-time dosimetry with radiochromic films. Sci. Rep. 9, 5307. https://doi.org/10.1038/s41598-019-41705-0

Church, C.C., 1995. The effects of an elastic solid surface layer on the radial pulsations of gas bubbles. J. Acoust. Soc. Am. 97, 1510–1521. https://doi.org/10.1121/1.412091

d'Errico, F., Nath, R., Nolte, R., 2000. A model for photon detection and dosimetry with superheated emulsions. Med. Phys. 27, 401–409. https://doi.org/10.1118/1.598844

D'Enrico, F., 2001. Radiation dosimetry and spectrometry with superheated emulsions. Nucl Instrum Methods Phys Res Sect B Beams Interact Mater At. 1 184, 229–254.

d'Errico (INVITED), F., 1999. Fundamental Properties of Superheated Drop (Bubble) Detectors. Radiat. Prot. Dosimetry 84, 55–62. https://doi.org/10.1093/oxfordjournals.rpd.a032796

Domenici, F., Brasili, F., Oddo, L., Cerroni, B., Bedini, A., Bordi, F., Paradossi, G., 2019. Long-term physical evolution of an elastomeric ultrasound contrast microbubble. J. Colloid Interface Sci. 540, 185–196. https://doi.org/10.1016/j.jcis.2018.12.110

Gaaz, T.S., Sulong, A.B., Akhtar, M.N., Kadhum, A.A.H., Mohamad, A.B., Al-Amiery, A.A., 2015. Properties and Applications of Polyvinyl Alcohol, Halloysite Nanotubes and Their Nanocomposites. Molecules 20, 22833–22847. https://doi.org/10.3390/molecules201219884

Glaser, D.A., 1952. Some Effects of Ionizing Radiation on the Formation of Bubbles in Liquids. Phys. Rev. 87, 665–665. https://doi.org/10.1103/PhysRev.87.665

Huang, Y., Vezeridis, A.M., Wang, J., Wang, Z., Thompson, M., Mattrey, R.F., Gianneschi, N.C., 2017. Polymer-Stabilized Perfluorobutane Nanodroplets for Ultrasound Imaging Agents. J. Am. Chem. Soc. 139, 15–18. https://doi.org/10.1021/jacs.6b08800

Heymans et al. Modulating ultrasound contrast generation from injectable nanodroplets for proton range verification by varaying the degree of superheat. Med. Phys. 2020. httos:// doi:…

Jiang, S., Liu, S., Feng, W., 2011. PVA hydrogel properties for biomedical application. J. Mech. Behav. Biomed. Mater. 4, 1228–1233. https://doi.org/10.1016/j.jmbbm.2011.04.005

Kripfgans, O.D., Fowlkes, J.B., Miller, D.L., Eldevik, O.P., Carson, P.L., 2000. Acoustic droplet vaporization for therapeutic and diagnostic applications. Ultrasound Med. Biol. 26, 1177–1189. https://doi.org/10.1016/S0301-5629(00)00262-3

Lacour, T., Guédra, M., Valier-Brasier, T., Coulouvrat, F., 2018. A model for acoustic vaporization dynamics of a bubble/droplet system encapsulated within a hyperelastic shell. J. Acoust. Soc. Am. 143, 23–37. https://doi.org/10.1121/1.5019467

Li, D.S., Schneewind, S., Bruce, M., Khaing, Z., O'Donnell, M., Pozzo, L., 2019. Spontaneous Nucleation of Stable Perfluorocarbon Emulsions for Ultrasound Contrast Agents. Nano Lett. 19, 173–181. https://doi.org/10.1021/acs.nanolett.8b03585

Loskutova, K., Grishenkov, D., Ghorbani, M., 2019. Review on Acoustic Droplet Vaporization in Ultrasound Diagnostics and Therapeutics [WWW Document]. BioMed Res. Int. https://doi.org/10.1155/2019/9480193

Mannaris, C., Yang, C., Carugo, D., Owen, J., Lee, J.Y., Nwokeoha, S., Seth, A., Teo, B.M., 2020. Acoustically responsive polydopamine nanodroplets: A novel theranostic agent. Ultrason. Sonochem. 60, 104782. https://doi.org/10.1016/j.ultsonch.2019.104782

Mohan, G., T P, A.H., A J, J., K M, S.D., Narayanasamy, A., Vellingiri, B., 2019. Recent advances in radiotherapy and its associated side effects in cancer—a review. J. Basic Appl. Zool. 80, 14. https://doi.org/10.1186/s41936-019-0083-5

Mohan, R., Mahajan, A., Minsky, B.D., 2013. New Strategies in Radiation Therapy: Exploiting the Full Potential of Protons. Clin. Cancer Res. 19, 6338–6343. https://doi.org/10.1158/1078-0432.CCR-13-0614

Mondal, P.K., Sarkar, R., Chatterjee, B.K., 2014. Characterization of R-134a superheated droplet detector for neutron detection. Appl. Radiat. Isot. 90, 1–7. https://doi.org/10.1016/j.apradiso.2014.02.024

Monde, M., 2015. Review of boiling explosion due to homogeneous nucleation in theoretical and experimental approach. J. Therm. Sci. Technol. 10, JTST0001–JTST0001. https://doi.org/10.1299/jtst.2015jtst0001

Mountford, P.A., Borden, M.A., 2016. On the thermodynamics and kinetics of superheated fluorocarbon phase-change agents. Adv. Colloid Interface Sci. 237, 15–27. https://doi.org/10.1016/j.cis.2016.08.007

Oddo, L., Cerroni, B., Domenici, F., Bedini, A., Bordi, F., Chiessi, E., Gerbes, S., Paradossi, G., 2017. Next generation ultrasound platforms for theranostics. J. Colloid Interface Sci. 491, 151–160. https://doi.org/10.1016/j.jcis.2016.12.030

Opalka, L., Granja, C., Hartmann, B., Jakubek, J., Jaekel, O., Martisikova, M., Pospisil, S., Solc, J., 2012. 3D measurement of the radiation distribution in a water phantom in a hadron therapy beam. J. Instrum. 7, C01085–C01085. https://doi.org/10.1088/1748-0221/7/01/C01085

Paradossi, G., Cavalieri, F., Chiessi, E., Spagnoli, C., Cowman, M.K., 2003. Poly(vinyl alcohol) as versatile biomaterial for potential biomedical applications. J. Mater. Sci. Mater. Med. 14, 687–691. https://doi.org/10.1023/A:1024907615244

Park, Y., Luce, A.C., Whitaker, R.D., Amin, B., Cabodi, M., Nap, R.J., Szleifer, I., Cleveland, R.O., Nagy, J.O., Wong, J.Y., 2012. Tunable Diacetylene Polymerized Shell Microbubbles as Ultrasound Contrast Agents. Langmuir 28, 3766–3772. https://doi.org/10.1021/la204510h

Parrales, M.A., Fernandez, J.M., Perez-Saborid, M., Kopechek, J.A., Porter, T.M., 2014. Acoustic characterization of monodisperse lipid-coated microbubbles: Relationship between size and shell viscoelastic properties. J. Acoust. Soc. Am. 136, 1077–1084. https://doi.org/10.1121/1.4890643

Parwaie, W., Refahi, S., Ardekani, M.A., Farhood, B., 2018. Different Dosimeters/Detectors Used in Small-Field Dosimetry: Pros and Cons. J. Med. Signals Sens. 8, 195–203. https://doi.org/10.4103/jmss.JMSS_3_18

Piermattei, A., Fidanzio, A., Azario, L., Grimaldi, L., D\textquotesingleOnofrio, G., Cilla, S., Stimato, G., Gaudino, D., Ramella, S., D\textquotesingleAngelillo, R., Cellini, F., Trodella, L., Russo, A., Iadanza, L., Zucca, S., Fusco, V., Napoli, N.D., Gambacorta, M.A., Balducci, M., Cellini, N., Deodato, F., Macchia, G., Morganti, A.G., 2007. Application of a practical method for the isocenter pointin vivodosimetry by a transit signal. Phys. Med. Biol. 52, 5101–5117. https://doi.org/10.1088/0031-9155/52/16/026

Reid, R.C., 1983. Rapid Phase Transitions from Liquid to Vapor, in: Wei, J., Bischoff, K.B., Drew, T.B., Seinfeld, J.H. (Eds.), Advances in Chemical Engineering. Academic Press, pp. 105–208. https://doi.org/10.1016/S0065-2377(08)60252-5

Reznik, N., Williams, R., Burns, P.N., 2011. Investigation of Vaporized Submicron Perfluorocarbon Droplets as an Ultrasound Contrast Agent. Ultrasound Med. Biol. 37, 1271–1279. https://doi.org/10.1016/j.ultrasmedbio.2011.05.001

Roy, S.C., 2001. Superheated liquid and its place in radiation physics. Radiat. Phys. Chem., 8th International Symposium on Radiation Physics - ISRP8 61, 271–281. https://doi.org/10.1016/S0969-806X(01)00250-X

Salla, J.M., Demichela, M., Casal, J., 2006. BLEVE: A new approach to the superheat limit temperature. J. Loss Prev. Process Ind. 19, 690–700. https://doi.org/10.1016/j.jlp.2006.04.004

Sánchez-Martín, D., Sanz, L., Ruoslahti, E., Alvarez-Vallina, L., 2013. In vivo selection of tumor-specific antibodies. Oncotarget 4, 1547.

Schindelin, J., 2012. Fiji: an open-source platform for biological-image analysis. https://doi.org/10.1038/nmeth.2019

Seitz, F., 1958. On the Theory of the Bubble Chamber. Phys. Fluids 1, 2–13. https://doi.org/10.1063/1.1724333

Sheeran, P.S., Luois, S., Dayton, P.A., Matsunaga, T.O., 2011a. Formulation and Acoustic Studies of a New Phase-Shift Agent for Diagnostic and Therapeutic Ultrasound. Langmuir 27, 10412–10420. https://doi.org/10.1021/la2013705

Sheeran, P.S., Luois, S.H., Mullin, L.B., Matsunaga, T.O., Dayton, P.A., 2012. Design of ultrasonically-activatable nanoparticles using low boiling point perfluorocarbons. Biomaterials 33, 3262–3269. https://doi.org/10.1016/j.biomaterials.2012.01.021

Sheeran, P.S., Matsunaga, T.O., Dayton, P.A., 2013a. Phase-transition thresholds and vaporization phenomena for ultrasound phase-change nanoemulsions assessed via high speed optical microscopy. Phys. Med. Biol. 58, 4513–4534. https://doi.org/10.1088/0031-9155/58/13/4513

Sheeran, P.S., Streeter, J.E., Mullin, L.B., Matsunaga, T.O., Dayton, P.A., 2013b. Toward Ultrasound Molecular Imaging With Phase-Change Contrast Agents: An In Vitro Proof of Principle. Ultrasound Med. Biol. 39, 893–902. https://doi.org/10.1016/j.ultrasmedbio.2012.11.017

Sheeran, P.S., Wong, V.P., Luois, S., Mcfarland, R.J., Ross, W.D., Feingold, S., Matsunaga, T.O., Dayton, P.A., 2011b. DECAFLUOROBUTANE AS A PHASE-CHANGE CONTRAST AGENT FOR LOW-ENERGY EXTRAVASCULAR ULTRASONIC IMAGING. Ultrasound Med. Biol. 37, 1518–1530. https://doi.org/10.1016/j.ultrasmedbio.2011.05.021

Sheeran, P.S., Yoo, K., Williams, R., Yin, M., Foster, F.S., Burns, P.N., 2017. More Than Bubbles: Creating Phase-Shift Droplets from Commercially Available Ultrasound Contrast Agents. Ultrasound Med. Biol. 43, 531–540. https://doi.org/10.1016/j.ultrasmedbio.2016.09.003

Toumia, Y., Cerroni, B., Domenici, F., Lange, H., Bianchi, L., Cociorb, M., Brasili, F., Chiessi, E., 2019. Phase Change Ultrasound Contrast Agents with a Photopolymerized Diacetylene Shell 12.

Verboven, E., D'Agostino, E., Callens, M., Pfeiffer, H., Verellen, D., D'hooge, J., Abeele, K.V.D., 2014. Ultrasound based dosimetry for radiotherapy: In-vitro proof of principle, in: 2014 IEEE International Ultrasonics Symposium. Presented at the 2014 IEEE International Ultrasonics Symposium, pp. 2265–2268. https://doi.org/10.1109/ULTSYM.2014.0564

Versluis, M., Stride, E., Lajoinie, G., Dollet, B., Segers, T., 2020. Ultrasound Contrast Agent Modeling: A Review. Ultrasound Med. Biol. 46, 2117–2144. https://doi.org/10.1016/j.ultrasmedbio.2020.04.014

Viessmann, O.M., Eckersley, R.J., Christensen-Jeffries, K., Tang, M.X., Dunsby, C., 2013. Acoustic super-resolution with ultrasound and microbubbles. Phys. Med. Biol. 58, 6447–6458.

Wilson, K., Homan, K., Emelianov, S., 2012. Biomedical photoacoustics beyond thermal expansion using triggered nanodroplet vaporization for contrast-enhanced imaging. Nat. Commun. 3, 618. https://doi.org/10.1038/ncomms1627

Zacek, V., 1994. Search for dark matter with moderately superheated liquids. Il Nuovo Cimento 1965-1970 107, 291–298. https://doi.org/10.1007/BF02781560

ACKNOWLEDGMENT

This work is conducted within the European project “AMPHORA” , funded by the European Union’s Horizon 2020 research and innovation program under contract n. **766456.**

The authors thank INFN IstitutoNazionale di Fisica Nucleare (Rome, Italy).

The authors thank the “Centre de Ressources du Cyclotron” of UCLouvain for the irradiation experiments.

CONFLICT OF INTEREST

The authors declare no conflict of interest.